Progress In Electromagnetics Research, Vol. 107, 129–146, 2010

EFFICIENT TIME-DOMAIN NOISE MODELING APPROACH FOR MILLIMETER-WAVE FETS

S. Asadi and M. C. E. Yagoub

SITE
University of Ottawa
800 King Edward, Ottawa, ON, K1N 6N5, Canada

Abstract—Based on the active coupled line concept, a novel approach for efficient noise performance modeling of millimeter-wave field-effect transistors is proposed. This distributed model considers the effect of wave propagation along the device electrodes, which can significantly affect the noise performance especially in the millimeter-wave range. By solving the multi-conductor transmission line equations, using the Finite-Difference Time-Domain technique, this procedure can accurately determine the noise correlation matrix of the transistor and then its noise performance.

1. INTRODUCTION

Efficient noise design of high frequency systems is critically based on accurate noise models of their internal components. As the core of modern communication systems, active devices should be carefully modeled for reliable system design.

In high frequencies, when the device physical dimensions become comparable to the wavelength, the input active transmission line has a different reactance from the output transmission line [1, 2], exhibiting different phase velocities for the input and output signals. So by increasing the frequency or device dimension the phase cancellation due to the phase velocity mismatching will affect the performance of the device [3]. Thus, a full-wave time-domain analysis involving distributed elements should be considered. However, this type of analysis is highly time consuming [4–7], even if different simulation time reduction techniques have been already proposed [8]. As a result,

Received 20 April 2010, Accepted 8 July 2010, Scheduled 4 August 2010
Corresponding author: S. Asadi (sasad063@uottawa.ca).

semi-distributed models such as the slice model, easily implemented in CAD routines, become a suitable alternative to overcome this limitation [9, 10]. However, by increasing the frequency, the slice model cannot precisely model the wave propagation effect and phase cancellation phenomena on the electrical performance. Therefore to achieve more accurate design in millimeter-wave applications, one needs to develop a more advanced distributed model.

In this paper, a distributed model is proposed [12]. It includes the effect of wave propagation along the electrodes more accurately than the semi distributed model although the CPU time of this model is a little greater than the slice model. Since a time domain analytical solution does not exist, a numerical approach should be used. Among all the existing methods, the Finite-Difference Time-Domain method (FDTD) was retained as one of the most widely used in this area [7–11].

2. SIGNAL MODELING OF HIGH-FREQUENCY FET

A typical millimeter-wave field effect transistor (FET) is shown in Fig. 1. It consists on three coupled electrodes (i.e., three active transmission lines).

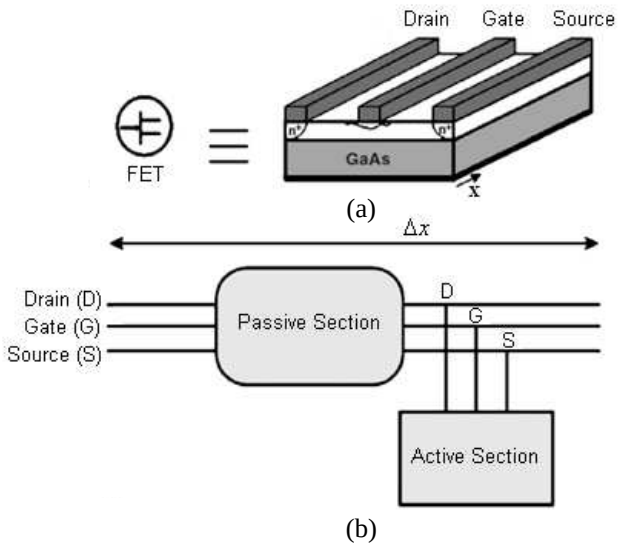

Figure 1. (a) 3D structure of FET used in millimeter-wave frequency. (b) A segment of distributed model along the wave propagation direction.

In the lower part of the microwave spectrum, the longitudinal electromagnetic (EM) field is very small in magnitude as compared to the transverse field [10, 12]. Therefore, a quasi-TEM mode can be considered to obtain the generalized active multi-conductor transmission line equation. An equivalent circuit of a section of the transistor is shown in Fig. 2. Each segment is represented by a 6-port equivalent circuit which combines a conventional FET small-signal equivalent circuit model with a distributed circuit to account for the coupled transmission line effect of the electrode structure where the all parameters are per unit length. By applying Kirchhoff's current laws to the left loop of the circuit in Fig. 2 with the condition $\Delta x \to 0$, we obtain the following system of equations [10, 12]:

$$\frac{\partial I_d(x,t)}{\partial x} + C_{11}\frac{\partial V_d(x,t)}{\partial t} - C_{12}\frac{\partial V_g(x,t)}{\partial t} - C_{13}\frac{\partial V_s(x,t)}{\partial t} + G_m V_g'(x,t) + G_{ds}(V_d(x,t) - V_s(x,t)) = 0 \quad (1)$$

$$\frac{\partial I_g(x,t)}{\partial x} + C_{22}\frac{\partial V_g(x,t)}{\partial t} - C_{12}\frac{\partial V_d(x,t)}{\partial t} + C_{gs}\frac{\partial V_g'(x,t)}{\partial t} = 0 \quad (2)$$

$$\frac{\partial I_s(x,t)}{\partial x} + C_{33}\frac{\partial V_s(x,t)}{\partial t} - C_{13}\frac{\partial V_d(x,t)}{\partial t} - C_{gs}\frac{\partial V_g'(x,t)}{\partial t} - G_m V_g'(x,t) + G_{ds}(V_s(x,t) - V_d(x,t)) = 0 \quad (3)$$

$$\frac{\partial V_d(x,t)}{\partial x} + R_d I_d(x,t) + L_{dd}\frac{\partial I_d(x,t)}{\partial t} + M_{gd}\frac{\partial I_g(x,t)}{\partial t} + M_{ds}\frac{\partial I_s(x,t)}{\partial t} = 0 \quad (4)$$

$$\frac{\partial V_g(x,t)}{\partial z} + R_g I_g(x,t) + L_{gg}\frac{\partial I_g(x,t)}{\partial t} + M_{gd}\frac{\partial I_d(x,t)}{\partial t} + M_{gs}\frac{\partial I_s(x,t)}{\partial t} = 0 \quad (5)$$

$$\frac{\partial V_s(x,t)}{\partial z} + R_s I_s(x,t) + L_{ss}\frac{\partial I_s(x,t)}{\partial t} + M_{ds}\frac{\partial I_d(x,t)}{\partial t} + M_{gs}\frac{\partial I_g(x,t)}{\partial t} = 0 \quad (6)$$

$$C_{11} = C_{dp} + C_{ds} + C_{dg} \quad C_{22} = C_{gp} + C_{dg}$$
$$C_{33} = C_{sp} + C_{ds} \quad C_{12} = C_{dg} \quad C_{13} = C_{ds}$$

where V_d, V_g, and V_s, are the drain, gate and source voltages, respectively, V_g' is the voltage across gate-source capacitor, while I_d, I_g, and I_s are the drain, gate and source currents, respectively. These variables are time-dependant and function of the position

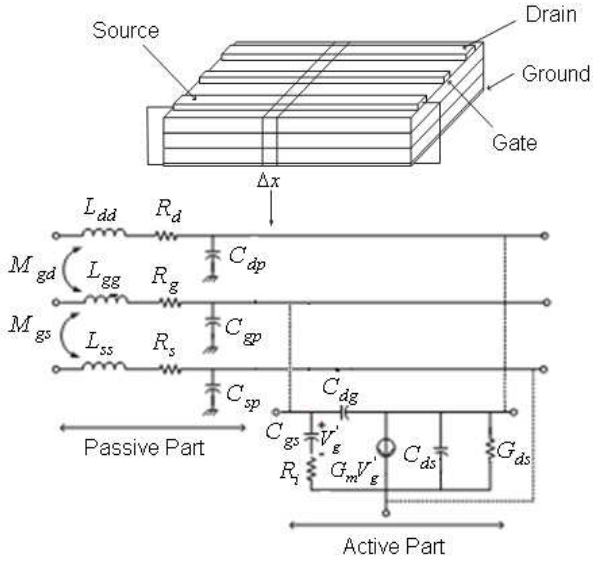

Figure 2. The different parts of a segment in the distributed model.

x along the device width. Also, M_{ds}, M_{gd}, and M_{gs} represent the mutual inductances between drain-source, gate-drain and gate-source, respectively; In the above system, we have an extra unknown parameter, i.e., the gate-source capacitance voltage V_g'. Therefore, the following equation should be included to complete the system of equations

$$V_g'(x,t) + V_s(x,t) + R_i C_{gs} \frac{\partial V_g'(x,t)}{\partial t} - V_g(x,t) = 0 \tag{7}$$

which can be then reformatted into two matrix equations

$$\frac{\partial}{\partial x}\begin{pmatrix} I_d(x,t) \\ I_g(x,t) \\ I_s(x,t) \\ 0 \end{pmatrix} + \frac{\partial}{\partial t}\begin{pmatrix} C_{11} & -C_{12} & -C_{13} & 0 \\ -C_{12} & C_{22} & 0 & C_{gs} \\ -C_{13} & 0 & C_{33} & -C_{gs} \\ 0 & 0 & 0 & R_i\, C_{gs} \end{pmatrix}\begin{pmatrix} V_d(x,t) \\ V_g(x,t) \\ V_s(x,t) \\ V_g'(x,t) \end{pmatrix}$$
$$+ \begin{pmatrix} G_{ds} & 0 & -G_{ds} & G_m \\ 0 & 0 & 0 & 0 \\ -G_{ds} & 0 & G_{ds} & -G_m \\ 0 & -1 & 1 & 1 \end{pmatrix}\begin{pmatrix} V_d(x,t) \\ V_g(x,t) \\ V_s(x,t) \\ V_g'(x,t) \end{pmatrix} = 0 \tag{8}$$

$$\frac{\partial}{\partial x}\begin{pmatrix} V_d(x,t) \\ V_g(x,t) \\ V_s(x,t) \end{pmatrix} + \frac{\partial}{\partial t}\begin{pmatrix} L_{dd} & M_{gd} & M_{ds} \\ M_{gd} & L_{gg} & M_{gs} \\ M_{ds} & M_{gs} & L_{ss} \end{pmatrix}\begin{pmatrix} I_d(x,t) \\ I_g(x,t) \\ I_s(x,t) \end{pmatrix} + \begin{pmatrix} R_d & 0 & 0 \\ 0 & R_g & 0 \\ 0 & 0 & R_s \end{pmatrix}\begin{pmatrix} I_d(x,t) \\ I_g(x,t) \\ I_s(x,t) \end{pmatrix} = 0 \tag{9}$$

3. NOISE MODELING OF HIGH-FREQUENCY FETS

The transmission line structure, exciting by noise equivalent sources distributed on the conductors as a new noise model of the high-frequency FET is shown in Fig. 3.

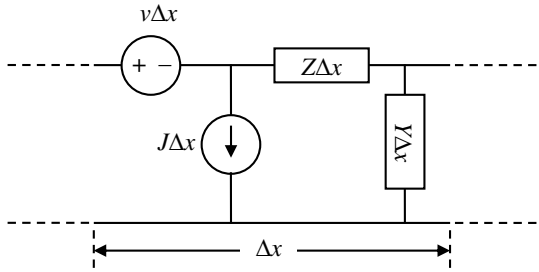

Figure 3. Differential subsection of an excited transmission line.

Applying Kirchhoff's laws in time domain leads to

$$\frac{\partial}{\partial x}\mathbf{I}' + \mathbf{C}\frac{\partial}{\partial t}\mathbf{V}' + \mathrm{G}\,\mathbf{V}' + \mathbf{j_n} = 0 \tag{10a}$$

$$\frac{\partial}{\partial x}\mathbf{V} + \mathbf{L}\frac{\partial}{\partial t}\mathbf{I} + \mathbf{R}\,\mathbf{I} + \mathbf{v_n} = 0 \tag{10b}$$

where

$$\mathbf{I}'(x,t) = \begin{pmatrix} I_d(x,t) \\ I_g(x,t) \\ I_s(x,t) \\ 0 \end{pmatrix} \qquad \mathbf{V}'(x,t) = \begin{pmatrix} V_d(x,t) \\ V_g(x,t) \\ V_s(x,t) \\ V_g'(x,t) \end{pmatrix}$$

$$\mathbf{I}(x,t) = \begin{pmatrix} I_d(x,t) \\ I_g(x,t) \\ I_s(x,t) \end{pmatrix} \qquad \mathbf{V}(x,t) = \begin{pmatrix} V_d(x,t) \\ V_g(x,t) \\ V_s(x,t) \end{pmatrix}$$

$$\mathbf{L} = \begin{pmatrix} L_{dd} & M_{gd} & M_{ds} \\ M_{gd} & L_{gg} & M_{gs} \\ M_{ds} & M_{gs} & L_{ss} \end{pmatrix} \qquad \mathbf{R} = \begin{pmatrix} R_d & 0 & 0 \\ 0 & R_g & 0 \\ 0 & 0 & R_s \end{pmatrix}$$

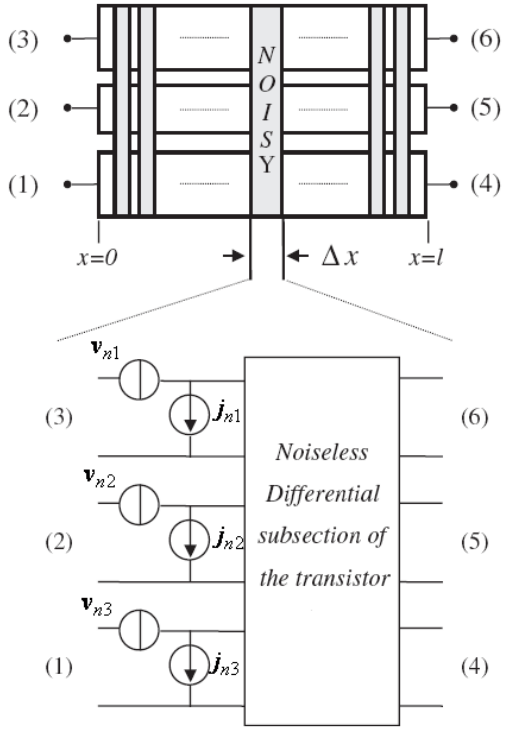

Figure 4. Noise-equivalent voltage and current sources.

$$\mathbf{C}=\begin{pmatrix} C_{11} & -C_{12} & -C_{13} & 0 \\ -C_{12} & C_{22} & 0 & C_{gs} \\ -C_{13} & 0 & C_{33} & -C_{gs} \\ 0 & 0 & 0 & R_i\,C_{gs} \end{pmatrix} \quad \mathbf{G}=\begin{pmatrix} G_{ds} & 0 & -G_{ds} & G_m \\ 0 & 0 & 0 & 0 \\ -G_{ds} & 0 & G_{ds} & -G_m \\ 0 & -1 & 1 & 1 \end{pmatrix}$$

Note that vectors $\mathbf{v_n}$ and $\mathbf{j_n}$ are the linear density of exciting voltage and current noise sources, respectively. To evaluate the noise sources, we considered a noisy FET subsection with gate width Δx, as shown in Fig. 4. Thus, the unit-per-length noise correlation matrix for chain representation of the transistor ($\mathbf{CA_{UPL}}$) can be deduced as [16–18]

$$\mathbf{CA_{UPL}} = \left\langle \begin{pmatrix} \mathbf{v_n} \\ \mathbf{j_n} \end{pmatrix} \begin{pmatrix} \mathbf{v_n} \\ \mathbf{j_n} \end{pmatrix}^{+} \right\rangle = \left\langle \begin{array}{cc} C_{11} & C_{12} \\ C_{21} & C_{22} \end{array} \right\rangle \tag{11}$$

where $\langle\,\rangle$ denotes the ensemble average and $+$ the transposed complex conjugate. According to the correlation matrix definition, we can calculate $\mathbf{v_n}$ and $\mathbf{j_n}$ knowing ($\mathbf{CA_{UPL}}$), to completely describe the

proposed FET noise model. Indeed, by solving (11), the noise parameters of the transistor can be obtained.

4. THE FDTD FORMULATION

The FDTD technique was used to solve the above equations. Applications of the FDTD method to the full-wave solution of Maxwell's equations have shown that accuracy and stability of the solution can be achieved if the electric and magnetic field solution points are chosen to alternate in space and be separated by one-half the position discretization, e.g., $\Delta x/2$, and to also be interlaced in time and separated by $\Delta t/2$ [13–15]. To incorporate these constraints into the FDTD solution of the transmission-line equations, we divided each line into N_x sections of length Δx, as shown in Fig. 5. Similarly, we divided the total solution time into segments of length Δt. In order to insure the stability of the discretization process and to insure second-order accuracy, we interlaced the $N_x + 1$ voltage points, V_1, V_2, ..., V_{Nx+1} and the N_x current points, I_1, I_2, ..., I_{Nx}. Each voltage and adjacent current solution points were separated by $\Delta x/2$. In addition, the time points are also interlaced, and each voltage time point and adjacent current time point were separated by $\Delta t/2$ [19, 20]. Then, (10) can lead to [12]

$$\begin{aligned}
&\frac{dI_k^{n+1/2}-dI_{k-1}^{n+1/2}}{\Delta x}+C_{11}\frac{dV_k^{n+1}-dV_k^n}{\Delta t}-C_{12}\frac{gV_k^{n+1}-gV_k^n}{\Delta t}\\
&-C_{13}\frac{sV_k^{n+1}-sV_k^n}{\Delta t}+G_m\frac{g'V_k^{n+1}+g'V_k^n}{2}\\
&+G_{ds}\frac{(dV_k^{n+1}+dV_k^n-sV_k^{n+1}-sV_k^n)}{2}+\sum_{m=1}^{Nx+1}\frac{n1v_m^{n+3/2}+n1v_m^{n+1/2}}{2}=0 \quad (12)\\
&\frac{gI_k^{n+1/2}-gI_{k-1}^{n+1/2}}{\Delta x}+C_{22}\frac{gV_k^{n+1}-gV_k^n}{\Delta t}-C_{12}\frac{dV_k^{n+1}-dV_k^n}{\Delta t}\\
&+C_{gs}\frac{g'V_k^{n+1}-g'V_k^n}{\Delta t}+\sum_{m=1}^{Nx+1}\frac{n2v_m^{n+3/2}+n2v_m^{n+1/2}}{2}=0 \quad (13)
\end{aligned}$$

$$\frac{sI_k^{n+1/2} - sI_{k-1}^{n+1/2}}{\Delta x} + C_{33}\frac{sV_k^{n+1} - sV_k^n}{\Delta t} - C_{13}\frac{dV_k^{n+1} - dV_k^n}{\Delta t}$$
$$-G_m\frac{g'V_k^{n+1} + g'V_k^n}{2} - G_{ds}\frac{(dV_k^{n+1} + dV_k^n - sV_k^{n+1} - sV_k^n)}{2}$$
$$+\sum_{m=1}^{Nx+1}\frac{n3v_m^{n+3/2} + n3v_m^{n+1/2}}{2} = 0 \tag{14}$$

$$\frac{dV_{k-1}^{n+1} - dV_k^{n+1}}{\Delta x} + R_d\frac{dI_k^{n+3/2} + dI_k^{n+1/2}}{2} + L_{dd}\frac{dI_k^{n+3/2} - dI_k^{n+1/2}}{\Delta t}$$
$$+M_{gd}\frac{gI_k^{n+3/2} - gI_k^{n+1/2}}{\Delta t} + M_{gs}\frac{sI_k^{n+3/2} - sI_k^{n+1/2}}{\Delta t}$$
$$+\sum_{m=1}^{Nx+1}\frac{n1j_m^{n+1} + n1j_m^n}{2} = 0 \tag{15}$$

$$\frac{gV_{k-1}^{n+1} - gV_k^{n+1}}{\Delta x} + R_g\frac{gI_k^{n+3/2} + gI_k^{n+1/2}}{2} + L_{gg}\frac{gI_k^{n+3/2} - gI_k^{n+1/2}}{\Delta t}$$
$$+M_{gd}\frac{dI_k^{n+3/2} - dI_k^{n+1/2}}{\Delta t} + M_{gs}\frac{sI_k^{n+3/2} - sI_k^{n+1/2}}{\Delta t}$$
$$+\sum_{m=1}^{Nx+1}\frac{n2j_m^{n+1} + n2j_m^n}{2} = 0 \tag{16}$$

$$\frac{sV_{k-1}^{n+1} - sV_k^{n+1}}{\Delta x} + R_s\frac{sI_k^{n+3/2} + sI_k^{n+1/2}}{2} + L_{ss}\frac{sI_k^{n+3/2} - sI_k^{n+1/2}}{\Delta t}$$
$$+M_{ds}\frac{dI_k^{n+3/2} - dI_k^{n+1/2}}{\Delta t} + M_{gs}\frac{gI_k^{n+3/2} - gI_k^{n+1/2}}{\Delta t}$$
$$+\sum_{m=1}^{Nx+1}\frac{n3j_m^{n+1} + n3j_m^n}{2} = 0 \tag{17}$$

Applying the finite difference approximation to (7) gives

$$R_i C_{gs}\frac{\left(gV_k^{n+1}\right)' - \left(gV_k^n\right)'}{\Delta t} + \frac{\left(gV_k^{n+1}\right)' - \left(gV_k^n\right)'}{2} + \frac{sV_k^{n+1} + sV_k^n}{2}$$
$$= \frac{gV_k^{n+1} + gV_k^n}{2} \tag{18}$$

with

$$ {}_dV_i^j = {}_dV((i-1)\Delta x, j\Delta t) \text{ and } {}_dI_i^j = {}_dI((i-1/2)\Delta x, j\Delta t) \text{ for the drain electrode} \quad (19a)$$

$$ {}_gV_i^j = {}_gV((i-1)\Delta x, j\Delta t) \text{ and } {}_gI_i^j = {}_gI((i-1/2)\Delta x, j\Delta t) \text{ for the gate electrode} \quad (19b)$$

$$ {}_sV_i^j = {}_sV((i-1)\Delta x, j\Delta t) \text{ and } {}_sI_i^j = {}_sI((i-1/2)\Delta x, j\Delta t) \text{ for the source electrode} \quad (19c)$$

and where k, m and n are integers. Solving these equations give the required recursion relations

$$V'^{n+1}_k = \left(\frac{C}{\Delta t}+\frac{G}{2}\right)^{-1}\left\{\left(\frac{C}{\Delta t}-\frac{G}{2}\right)V'^{n}_k - \frac{I'^{n+1/2}_k - I'^{n+1/2}_{k-1}}{\Delta x} + \frac{\Delta x}{2}\sum_{m=1}^{Nx+1}\left(j_m^{n+1}+j_m^n\right)\right\} \quad (20)$$

$$I_k^{n+3/2} = \left(\frac{L}{\Delta t}+\frac{R}{2}\right)^{-1}\left\{\left(\frac{L}{\Delta t}-\frac{R}{2}\right)I_k^{n+1/2} - \frac{V_{k+1}^{n+1}-V_k^{n+1}}{\Delta x} + \frac{\Delta x}{2}\sum_{m}^{Nx+1}\left(v_m^{n+3/2}+v_m^{n+1/2}\right)\right\} \quad (21)$$

Superposing all the distributed noise sources is equivalent to a summation in (20) and (21) over the gate width for $m = 1, \ldots, N_x+1$.

Because of its simplicity, the leap-frog method was used to solve the above equations. First the voltages along the line were solved for a fixed time using (20) then the currents were determined using (21). The solution starts with an initially relaxed line having zero voltage and current [13, 14].

5. NOISE CORRELATION MATRIX OF TRANSISTOR

To find the noise correlation matrix for admittance representation of the transistor as a noisy six-port active network (as in Fig. 2), the values of port currents should be determined when they are all assumed short-circuited simultaneously. Equation (20) for $k = 0$ and $k = N_x+1$

becomes

$$V_1'^{n+1} = \left(\frac{C}{\Delta t} + \frac{G}{2}\right)^{-1} \left\{ \left(\frac{C}{\Delta t} - \frac{G}{2}\right) V_1'^{n} - \frac{I_1'^{n+1/2} - I_0'^{n+1/2}}{\Delta x/2} + \frac{\Delta x}{2} \sum_{m=1}^{Nx+1} \left(j_m^{n+1} + j_m^n\right) \right\} \tag{22}$$

$$V_{Nx+1}'^{n+1} = \left(\frac{C}{\Delta t} + \frac{G}{2}\right)^{-1} \left\{ \left(\frac{C}{\Delta t} - \frac{G}{2}\right) V_{Nx+1}'^{n} - \frac{I_{Nx+1}'^{n+1/2} - I_{Nx}'^{n+1/2}}{\Delta x/2} + \frac{\Delta x}{2} \sum_{m=1}^{Nx+1} \left(j_m^{n+1} + j_m^n\right) \right\} \tag{23}$$

By considering Fig. 3, this equation requires that we replace Δx with $\Delta x/2$ only for $k = 1$ and $k = N_x + 1$.

In order to determine the transistor noise parameters, we set the input voltage source as zero ($V_s = 0$) [8, 9]. Referring Fig. 6, we denoted the currents at the source point ($x = 0$) as I_0 and at the load point ($x = L$) as I_{Nx+1}. By substituting this notation into (22) we obtain

$$\begin{pmatrix} I_{0d} \\ I_{0g} \\ I_{0s} \end{pmatrix} = \begin{pmatrix} \frac{V_{1d}^n - V_{1d}^{n+1}}{2R_{sd}} & 0 & 0 \\ 0 & \frac{V_{1g}^n - V_{1g}^{n+1}}{2R_{sg}} & 0 \\ 0 & 0 & \frac{V_{1s}^n - V_{1s}^{n+1}}{2R_{ss}} \end{pmatrix} \tag{24}$$

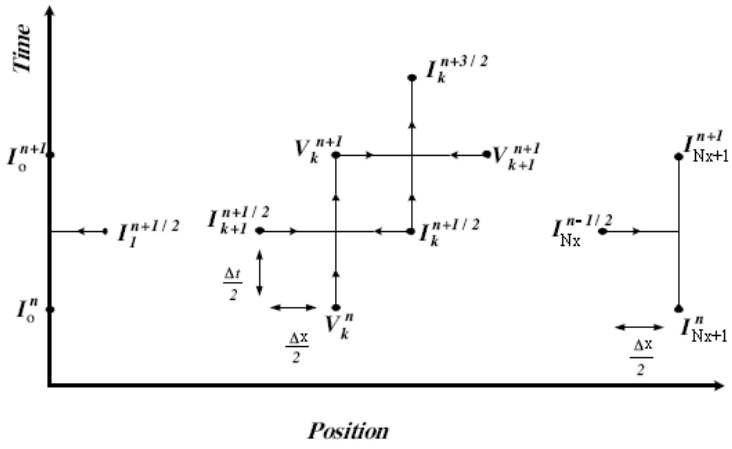

Figure 5. Relation between the spatial and temporal discretization to achieve second-order accuracy in the discretization of the derivatives.

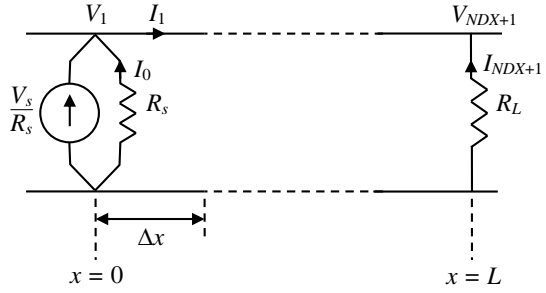

Figure 6. Voltage and current solution points. Spatial discretization of the line showing location of the interlaced points.

Similarly, we imposed the terminal constraint at $x = L$ by substituting I_{Nx+1} into (23) as follow:

$$\begin{pmatrix} I_{Nx+1,d} \\ I_{Nx+1,g} \\ I_{Nx+1,s} \end{pmatrix} = \begin{pmatrix} \frac{V^n_{Nx+1,d} - V^{n+1}_{Nx+1,d}}{2R_{Ld}} & 0 & 0 \\ 0 & \frac{V^n_{Nx+1,g} - V^{n+1}_{Nx+1,g}}{2R_{Lg}} & 0 \\ 0 & 0 & \frac{V^n_{Nx+1,s} - V^{n+1}_{Nx+1,s}}{2R_{Ls}} \end{pmatrix} \quad (25)$$

To determine the currents I_1 and I_{Nx} at short-circuited ports ($x = 0$ and $x = L$), we set $V_1 = V_{Nx+1} = 0$. The finite difference approximation of (21) for $k = 1$ and $k = N_x$ can be then written as (26) and (27), respectively.

$$I_1^{n+3/2} = \left(\frac{L}{\Delta t} + \frac{R}{2}\right)^{-1} \left\{ \left(\frac{L}{\Delta t} - \frac{R}{2}\right) I_1^{n+1/2} - \frac{V_2^{n+1}}{\Delta x} + \frac{\Delta x}{2} \sum_{m=1}^{Nx+1} \left(v_m^{n+3/2} + v_m^{n+1/2}\right) \right\} \quad (26)$$

$$I_{Nx}^{n+3/2} = \left(\frac{L}{\Delta t} + \frac{R}{2}\right)^{-1} \left\{ \left(\frac{L}{\Delta t} - \frac{R}{2}\right) I_{Nx}^{n+1/2} - \frac{V_{Nx}^{n+1}}{\Delta x} + \frac{\Delta x}{2} \sum_{m=1}^{Nx+1} \left(v_m^{n+3/2} + v_m^{n+1/2}\right) \right\} \quad (27)$$

Replacing $I_1^{n+1/2}$ and $I_{Nx}^{n+1/2}$ into (26) and (27), respectively, leads to

short-circuit currents at input and output terminals.

$$I_1^{n+3/2} = \left(\frac{L}{\Delta t}+\frac{R}{2}\right)^{-1}\left\{\left(\frac{L}{\Delta t}-\frac{R}{2}\right)\left(\frac{\Delta x}{2}\right)^2\sum_{m=1}^{Nx+1}\left(j_m^{n+1}+j_m^n\right) + \frac{\Delta x}{2}\sum_{m=1}^{Nx+1}\left(v_m^{n+3/2}+v_m^{n+1/2}\right)-\frac{V_2^{n+1}}{\Delta x}\right\} \tag{28}$$

$$I_{Nx}^{n+3/2} = \left(\frac{L}{\Delta t}+\frac{R}{2}\right)^{-1}\left\{\left(\frac{L}{\Delta t}-\frac{R}{2}\right)\left(\frac{\Delta x}{2}\right)^2\sum_{m=1}^{Nx+1}\left(j_m^{n+1}+j_m^n\right) + \frac{\Delta x}{2}\sum_{m=1}^{Nx+1}\left(v_m^{n+3/2}+v_m^{n+1/2}\right)-\frac{V_{Nx}^{n+1}}{\Delta x}\right\} \tag{29}$$

Finally, the currents of the short-circuited ports can be determined as

$$\begin{bmatrix} I_1^{n+1/2} \\ I_{Nx}^{n+3/2}\end{bmatrix} \cong \begin{bmatrix} A & B \\ A & B\end{bmatrix}\begin{bmatrix} \sum_{m=1}^{Nx+1}\left(j_m^{n+1}+j_m^n\right) \\ \sum_{m=1}^{Nx+1}\left(v_m^{n+3/2}+v_m^{n+1/2}\right)\end{bmatrix} = K\begin{bmatrix} \sum_{m=1}^{Nx+1}\left(j_m^{n+1}+j_m^n\right) \\ \sum_{m=1}^{Nx+1}\left(v_m^{n+3/2}+v_m^{n+1/2}\right)\end{bmatrix} \tag{30}$$

with

$$A=\left(\frac{L}{\Delta t}+\frac{R}{2}\right)^{-1}\left\{\left(\frac{L}{\Delta t}-\frac{R}{2}\right)\left(\frac{\Delta x}{2}\right)^2\right\} \quad B=\left(\frac{L}{\Delta t}+\frac{R}{2}\right)^{-1}\left(\frac{\Delta x}{2}\right)$$

The admittance noise correlation matrix of the six-port FET noise model is then equal to

$$CY_{tr} = \left\langle \begin{bmatrix} I_1^{n+1/2} \\ I_1^{n+3/2}\end{bmatrix}\begin{bmatrix} I_1^{n+1/2} \\ I_1^{n+3/2}\end{bmatrix}^+ \right\rangle = \left\langle \left(K\begin{bmatrix}\sum j_n \\ \sum v_n\end{bmatrix}\right)\left(K\begin{bmatrix}\sum j_n \\ \sum v_n\end{bmatrix}\right)^+ \right\rangle = K \times CA_{UPL} \times K^+ \tag{31}$$

6. NUMERICAL RESULTS

The proposed approach was used to model a sub micrometer-gate FET transistor (NE710). The device has a $0.3 \times 560\,\mu\text{m}$ gate. The input

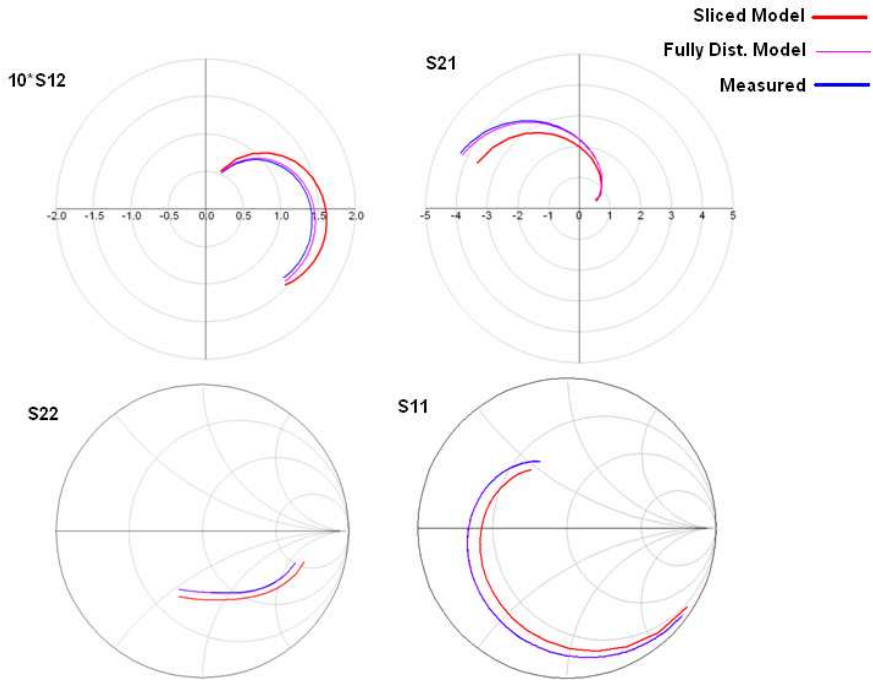

Figure 7. Comparison between S-parameters of NE710 for sliced, fully distributed model and measurements.

and output nodes were connected to the beginning of the gate electrode and at the end of the drain electrode, respectively. The transistor was biased at $V_{ds} = 3\,\mathrm{V}$ and $I_{ds} = 10\,\mathrm{mA}$ [21]. The obtained S-parameters of the transistor over a frequency range of 1–26 GHz from the sliced model, the proposed fully distributed model and measurements are plotted in Fig. 7.

As expected, our distributed model is more close to measurements than the slice model [9], especially at the upper part of the frequency spectrum, when the device physical dimensions are comparable to the wavelength. This is due to the fact that our fully distributed model is based on the full-wave equation while the slice model is based on an electrical circuit model. Fig. 8 shows the noise figure obtained for three different sets of data.

Thus, the proposed wave analysis can be applied for accurate noise analysis of FET circuits. To further prove the accuracy of the proposed wave approach in noise analysis, our results were successfully compared to measurements as well as to those obtained by the sliced

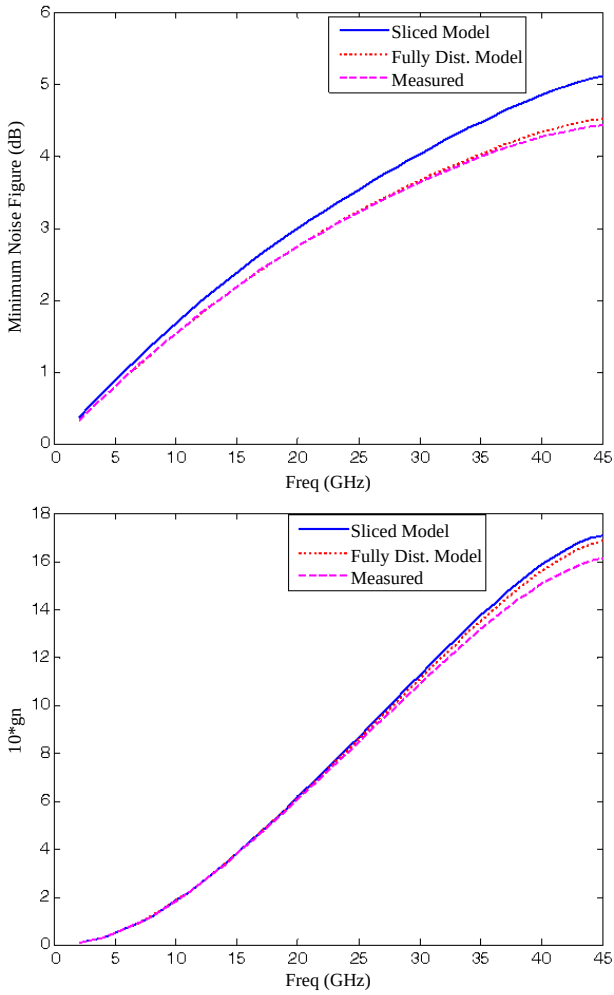

Figure 8. Comparison between normalized equivalent noise admittance and noise figure for sliced, fully distributed model and measurements.

model, highlighting the advantage of our model over this later (Fig. 9). Figs. 10(a) and 10(b) show the minimum noise figure and normalized equivalent noise admittance vs. the transistor gate width, respectively.

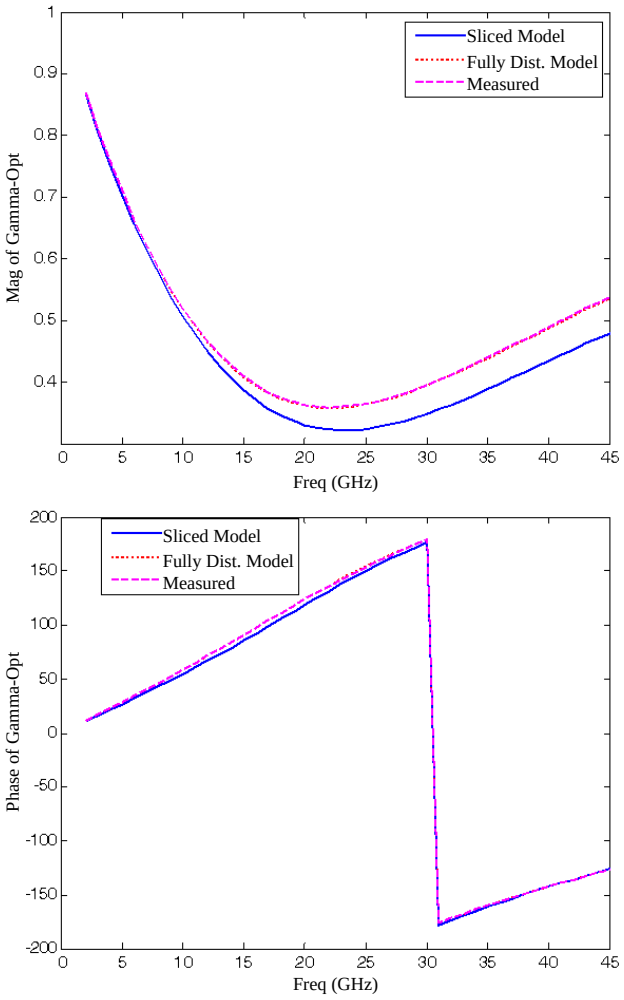

Figure 9. Comparison between the results of slice modeling, fully distributed model and measured values of amplitude and the phase of optimum reflection coefficient.

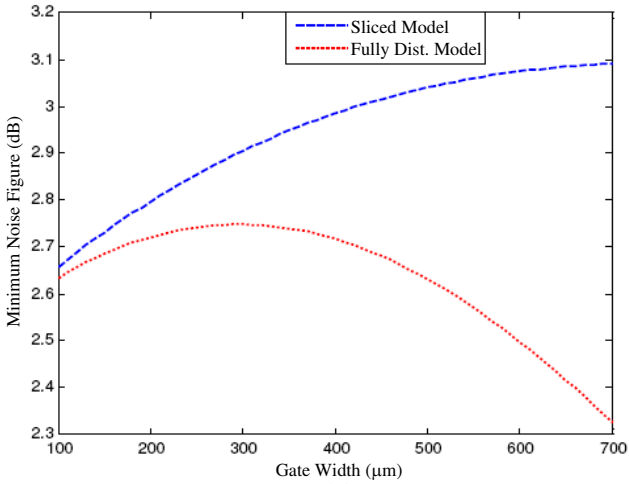

Figure 10. (a) Comparison between noise figure for sliced and fully distributed model versus gate width. (b) Comparison between normalized equivalent noise admittance for sliced and fully distributed model versus gate width.

7. CONCLUSION

A new modeling approach for noise analysis of high frequency transistors was presented. This method can accurately take into account the effect of wave propagation along the device electrodes. The promising model can be applied to solve issues related to simultaneous signal and noise analysis, as well as in modeling traveling wave FETs in which the gate width is much higher than that of a usual FET.

REFERENCES

1. Imtiaz, S. M. S. and S. M. Ghazaly, "Global modeling of millimeter-wave circuits: Electromagnetic simulation of amplifiers," *IEEE Trans. Microwave Theory Tech.*, Vol. 45, 2208–2216, 1997.
2. Li, J., L. X. Guo, and H. Zeng, "FDTD investigation on bistatic scattering from a target above two-layered rough surfaces using UPML absorbing condition," *Progress In Electromagnetics Research*, Vol. 88, 197–211, 2008.
3. Lei, J. Z., C. H. Liang, W. Ding, and Y. Zhang, "EMC analysis of antennas mounted on electrically large platforms with parallel FDTD method," *Progress In Electromagnetics Research*, Vol. 84, 205–220, 2008.
4. Wang, M. Y., J. Xu, J. Wu, B. Wei, H. L. Li, T. Xu, and D. B. Ge, "FDTD study on wave propagation in layered structures with biaxial anisotropic metamaterials," *Progress In Electromagnetics Research*, Vol. 81, 253–265, 2008.
5. Mirzavand, R., A. Abdipour, G. Moradi, and M. Movahhedi, "Full-wave semiconductor devices simulation using adi-FDTD method," *Progress In Electromagnetics Research M*, Vol. 11, 191–202, 2010.
6. Goasguen, S., M. Tomeh, and S. M. Ghazaly, "Electromagnetic and semiconductor device simulation using interpolating wavelets," *IEEE Trans. Microwave Theory Tech.*, Vol. 49, 2258–2265, 2001.
7. Hussein, Y. A. and S. M. Ghazaly, "Modeling and optimization of microwave devices and circuits using genetic algorithms," *IEEE Trans. Microwave Theory Tech.*, Vol. 52, 329–336, 2004.
8. Movahhedi, M. and A. Abdipour, "Efficient numerical methods for simulation of high-frequency active devices," *IEEE Trans. Microwave Theory Tech.*, Vol. 54, 2636–2645, 2006.
9. Abdipour, A. and G. Moradi, "A CAD-oriented simultaneous

signal and noise modeling and analysis of mm-wave FET structures," *AEU — Int. J. of Electronics and Communications*, Vol. 58, 65–71, 2004.

10. Abdelaziz, A. F., T. M. Abuelfadl, and O. L. Elsayed, "Realization of composite right/left-handed transmission line using coupled lines," *Progress In Electromagnetics Research*, Vol. 92, 299–315, 2009.
11. Tafove, A., *Computational Electrodynamics: The Finite Difference Time-domain Method*, Artech House, Norwood, 1996.
12. Gaoua, S., S. Asadi, M. C. E. Yagoub, and F. A. Mohammadi, "CAD tools for efficient RF/microwave transistor modeling and circuit design," *Analog Integrated Circuits and Signal Processing J.*, Vol. 63, 59–70, 2010.
13. Cheldavi, A., D. Ansari, and M. Khalaj-Amirhosseini, "Electromagnetic coupling to circulant symmetric multi-conductor microstrip line," *Progress In Electromagnetics Research*, Vol. 49, 189–201, 2004.
14. Pospieszalski, M. W., "Modeling of noise parameters of MESFETs and MODFETs and their frequency and temperature dependence," *IEEE Trans. Microwave Theory Tech.*, Vol. 37, 385–388, 1989.
15. Fu, Y., K. Li, and F. Kong, "Analysis of the optical transmission through the metal plate with slit array," *Progress In Electromagnetics Research*, Vol. 82, 109–125, 2008.
16. Dobrowolski, J. A., *Introduction to Computer Methods for Microwave Circuit Analysis and Design*, Artech House, Boston, 1991.
17. Dobrowolski, J. A., *Computer-aided Analysis, Modeling, and Design of Microwave Networks (Wave Approach)*, Artech House, Boston, 1996.
18. Movahhedi, M. and A. Abdipour, "Accelerating the transient simulation of semiconductor devices using filter-bank transforms," *Int. J. Numer. Mod.*, Vol. 19, 4767, 2006.
19. Kung, F. and H. T. Chuah, "A finite-difference time-domain (FDTD) software for simulation of printed circuit board (PCB) assembly," *Progress In Electromagnetics Research*, Vol. 50, 299–335, 2005.
20. Khalaj-Amirhosseini, M., "Analysis of nonuniform transmission lines using the equivalent sources," *Progress In Electromagnetics Research*, Vol. 71, 95–107, 2007.
21. http://www.nec.com.